



Design, synthesis, and biological activity of TLR7-based compounds for chemotherapy-induced alopecia

Jincheng Yang¹ · Kun Chen² · Bin Wang³ · Liudi Wang³ · Shuya Qi¹ · Weihua Wang¹

Received: 29 March 2019 / Accepted: 13 May 2019
© Springer Science+Business Media, LLC, part of Springer Nature 2019

Summary

Hair loss is a common dermatosis symptom and side-effect in cancer chemotherapeutics. Imiquimod application at mid and late telogen activated the hair follicle stem cells leading to premature hair cycle entry. Based on quinoline structure, a newly synthesized compound 6b displayed proliferation activity in vitro and in vivo through branch chain replacement and triazole ring cyclization. Toll-like receptors (TLRs) are also critical mediators of the immune system, and their activation is linked to various diseases. The present study aimed to expand new agonists within co-crystallization of TLR7 (PDB code: 5GMH); however, biological assays of NF- κ B activity and NO-inhibition indicated that five selected compounds were TLR7 antagonists. Molecular docking indicated the binding mode differences: antagonists binding TLR7 in a different direction and interacting with adjacent TLR7 with difficulty in forming dimers.

Keywords TLR7 · Hair follicle stem cell · Chemotherapy-induced alopecia · Antagonist · Synthesis

Introduction

Hair loss is both a common dermatosis condition and a side-effect in patients undergoing chemotherapeutic treatment for cancer. Hair loss experience causes feelings of distorted self-image and low self-esteem, and may display symptoms of anxiety and depression in sufferers [1]. Alopecia is a common skin disease in patients with neoplastic medical behaviors [2, 3] affecting all genders and age groups [4]. Chemotherapy-induced alopecia (CIA) is frequently described as one of the most distressing aspects of cancer treatments [5].

Although CIA is usually reversible, new hair shows graying and/or changes in the structure and texture, and the hair growth rate might also be significantly reduced [6]. In several patients, the regrown hair shows altered color and/or structure and texture. In some cases, the hair density may be reduced [7]. Permanent CIA could result from irreversible hair follicle stem cell destruction in the hair bulge [1] or disruption of signaling to the secondary hair germination [8].

Hair follicles undergo repeated cycles of anagen (growth), catagen (regression), and telogen (quiescence) throughout the life in mammals following morphogenesis [9]. Additionally, the degree of damage to the hair follicle stem cell (HFSC) determines whether the CIA is reversible; if chemotherapy only has effects on the bulge of the stem cells (at the middle of hair shaft), alopecia is reversible, while if the bulb is affected (at the bottom of hair shaft), alopecia is irreversible. Currently, HFSC proliferation is used for the prevention or treatment of CIA. Predominantly, CIA affects the highly proliferative matrix keratinocytes of anagen hair follicles that are located in the hair bulb. However, damaged HFSCs could also lead to permanent hair loss [10].

Imiquimod (Toll-like receptor-7 (TLR7) agonist) is a quinoline derivative and applied to mid and late telogen-activated HFSCs, which leads to premature hair cycle entry (anagen) [11]. In 2007, Letada et al. presented a case of a 15-year-old girl with alopecia universalis since the age of 8 years, who

✉ Jincheng Yang
Yangjc@cicams.ac.cn

¹ Department of Pharmacy, National Cancer Center/National Clinical Research Center for Cancer/Cancer Hospital, Chinese Academy of Medical Sciences and Peking Union Medical College, Panjiayuan Nanli 17, Chaoyang Qu, Beijing 100021, China

² State Key Laboratory of Molecular Oncology/Department of Immunology, National Cancer Center/National Clinical Research Center for Cancer/Cancer Hospital, Chinese Academy of Medical Sciences and Peking Union Medical College, Beijing 100021, China

³ Clinical Stem Cell Center, The Affiliated Drum Tower Hospital of Nanjing University Medical School, Nanjing 210008, China

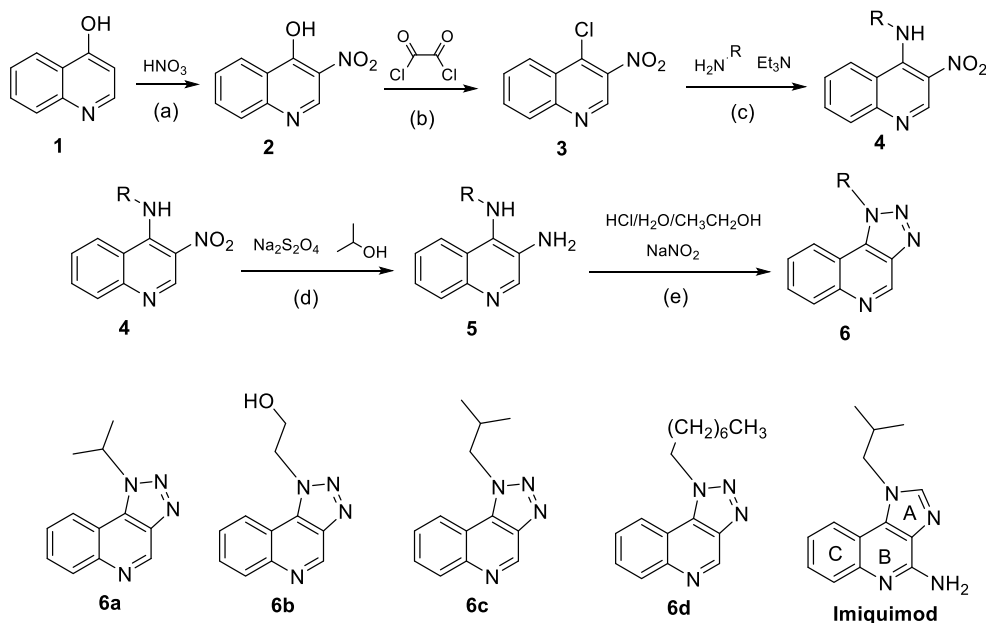
experienced transient hair growth after topical application of imiquimod [12].

Paus and Cotsarelis reported the development of drugs that shield the rapidly proliferating bulb cells from chemotherapeutic damage and protect the stem cells from irreversible damage by the infiltration of autoimmune inflammatory cells or ionizing radiation [13]. These studies on CIA-treating drugs reduced the social and psychological effects accompanying tumor therapy, and prevention of hair loss due to chemotherapy benefitted a large number of patients undergoing cancer treatment. Herein, we reported a new series of synthesized quinoline derivatives and prepared a new compound for furnishing valuable information on HFSC-proliferation drug design models.

Results

Compound synthesis

In this study, quinoline derivatives were synthesized from 4-hydroxyquinoline. The key step was the introduction of



Scheme 1 Synthesis of quinoline derivatives and structure of imiquimod. Reagents and conditions: (a) conc HNO₃, propanoic acid, ref. 1.5 h; (b) Oxalyl chloride, DCM, 40 °C, 0.5 h; (c) Amines, TEA, CH₃OH, rt. 0.5–2 h; (d) Na₂S₂O₄, isopropanol, H₂O, ref. 2 h; (e) NaNO₂, HCl, H₂O, EtOH, ice-water bath, overnight. ① Compound **6a**: mp:114–116°C. ¹H-NMR(CDCl₃, 400MHz): σ (ppm) 9.57(s, 1H), 8.35(t, 2H, $J=7$ Hz), 7.85(td, 1H, $J_1=7.8$ Hz, $J_2=1.2$ Hz), 7.76(td, 1H, $J_1=7.8$ Hz, $J_2=1.2$ Hz), 5.50(quint, 1H, $J=6.8$ Hz), 1.92(d, 6H, $J=6.8$ Hz). IR (KBr): 3065, 2993, 2942, 1620, 1578, 1521, 1451, 1383, 1260, 1091, 768 cm⁻¹. MS (EI+) m/z: 235 (M+Na⁺). HRMS m/s calculated for C₁₂H₁₂N₄+H⁺ 235.0954, found 235.0964. ② Compound **6b**: mp:170–172°C. ¹H-NMR(CDCl₃, 400MHz): σ (ppm) 9.44(s, 1H), 8.42(dd, 1H, $J_1=8.4$ Hz, $J_2=0.8$ Hz), 8.27(d, 1H, $J=8.4$ Hz), 7.83(td, 1H, $J_1=7.6$ Hz, $J_2=1.2$ Hz), 7.50(td, 1H, $J_1=7.8$ Hz, $J_2=1.2$ Hz), 5.17(t, 2H, $J=5.2$ Hz), 4.45(t, 2H, $J=5$ Hz). IR (KBr): 3292, 3070, 3007,

various amine groups onto the main quinoline structure. Then, the nitro-group was reduced into the amino-group, and the final cyclization was complicated with NaNO₂ in an ice-water bath (Scheme 1).

Lipophilicity values

Lipophilicity is a significant physicochemical property determining the distribution, bioavailability, metabolic activity, and elimination, and hence, essential for comparison among the synthetic compounds. The lipophilicity of the synthesized derivatives was determined experimentally from RP-TLC (Reversed Phase Thin Layer Chromatography) as R_M values and compared with the corresponding theoretically calculated Clog *P*-values in n-octanol-buffer [14]. Compound 6b presented minimal values (Table 1), indicating that lower the lipophilicity value, higher the biological activity.

HFSC proliferation in vitro

The in vivo pilot test demonstrated that only compound 6b among the four target compounds (6a–6d) promoted hair

2941, 2851, 1621, 1586, 1524, 1454, 1388, 1323, 1166, 1069, 761 cm⁻¹. MS (EI+) m/z: 237 (M+Na⁺). HRMS m/s calculated for C₁₁H₁₀N₄O+Na⁺ 237.0747, found 237.0745. ③ Compound **6c**: mp:66–68°C. ¹H-NMR(CDCl₃, 400MHz): σ (ppm) 9.55(s, 1H), 8.35(d, 1H, $J=8$ Hz), 8.23(d, 1H, $J=8$ Hz), 7.84(t, 1H, $J=7.4$ Hz), 7.76(t, 1H, $J=7.2$ Hz), 4.85(d, 2H, $J=7.2$ Hz), 2.48(quint, 1H, $J=6.4$ Hz), 1.08(d, 6H, $J=6.4$ Hz). IR (KBr): 3064, 3016, 2964, 2935, 2906, 2875, 1624, 1523, 1459, 1389, 1370, 1322, 1178, 761 cm⁻¹. MS (ES+) m/z: 227 (M+H⁺). HRMS m/s calculated for C₁₃H₁₄N₄+Na⁺ 249.1111, found 249.1115. ④ Compound **6d**: mp:168–170°C. ¹H-NMR(CDCl₃, 400MHz): σ (ppm) 9.68(s, 1H), 8.95(s, 1H), 8.42(d, 1H, $J=7.2$ Hz), 8.09–8.03(m, 2H), 5.15(t, 2H, $J=7.2$ Hz), 2.17(t, 2H, $J=7.2$ Hz), 1.27(s, 10H), 0.87(t, 3H, $J=6.6$ Hz). IR (KBr): 3058, 2925, 1646, 1611, 1590, 1511, 1462, 1442, 1317, 776, 724 cm⁻¹. MS (ES+) m/z: 283 (M+H⁺). HRMS m/s calculated for C₁₇H₂₂N₄+H⁺ 283.1917, found 283.1924

Table 1 Lipophilicity values: R_M , $C_{\log P}$, and $\log P$

	Imiquimod	6a	6b	6c	6d
^a $R_M=[(1/R_p)-1]$	0.879	0.176	-0.368	0.301	0.954
^b $C_{\log P}$	3.236	2.435	1.004	3.054	5.300
^c $\log P=C_o/C_w$	2.077	1.647	0.534	2.052	2.714

^a R_M values are the average of 10 measurements. ^b $C_{\log P}$: Theoretical values. ^c $\log P$: experimental values

follicle proliferation in normal mouse skin. Thus, the following assays were designed on compound 6b.

Mouse hair follicle stem cells were prepared according to the authoritative isolation method [15] (Fig. 1). The potential markers for hair follicle stem cells include $\beta 1$ -integrin, keratin 19, $\alpha 6$ -integrin, CD71, p63, and CD34 [16, 17]. In the present study, PE-anti-mouse CD34 antibody and FITC-anti-mouse $\beta 1$ integrin were selected to identify HFSCs. The results of testing mixed antibodies or single antibody of $\beta 1$ and CD34 did not reveal any overlap in flow cytometry, indicating the presence of stem cells (Fig. 2).

Hair follicle proliferation in vivo

The effects of compound cream treatment on the skin consisted of three components: normal mice, acute toxicity, and chemotherapy treatment. The results of treated and untreated sides of the skins of one mouse were compared.

Normal mice group: H-E (hematoxylin-eosin) staining showed that the number of hair follicles in the compound-treated group was higher than that in the control group (Fig. 3). Acute toxicity is a crucial assay for studying the drug effect with respect to high drug density and dosage on an organism. The current results did not show any abnormality on the skin, mouse body, as well as the daily life of the animal, while the number of hair follicles increased markedly (Fig. 4).

Next, the chemotherapy treatment adopted CYP (cyclophosphamide) and DOX (Doxorubicin) as both agents exerted common anti-neoplastic effects in breast cancer

treatment. C57BL/6 and BALB/c mice were selected as two experimental models. The first stage of chemotherapy assays was injecting the anti-neoplastic drug into normal mice simultaneously when both sides of the hair were depilated, spreading compound cream on the right back side and control-cream on the left back side. The compound-treated groups showed higher hair follicle density than the control groups (Figs. 5, 6, 7, 8). The second stage was injecting the agents into female mice established as breast cancer model with 4 T1 cells. Similar to the first stage, the two sides of the skin were collected, and the hair follicle examined. In addition to the difference in the hair follicle density, the data also indicated weak hair of mice in the CYP + DOX group (Fig. 9).

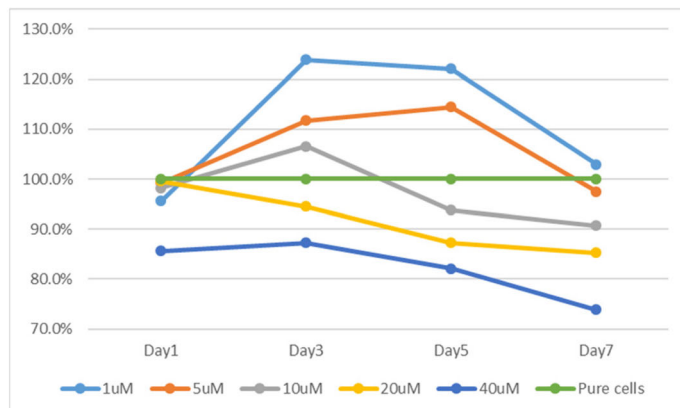
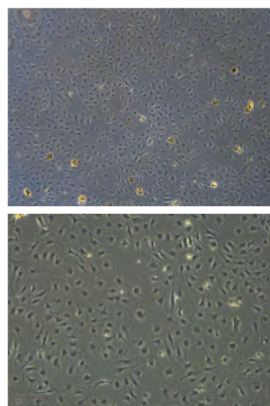
The breast cancer patients underwent various chemotherapeutic regimens consisting mainly of CTX (cyclophosphamide), DOX (doxorubicin), or 5-FU (5-fluorouracil), as adjuvant therapy after the surgery. 4 T1 is a commonly used mouse triple-negative breast cancer (TNBC) cell line [18]. When injected into BALB/c mice, 4 T1 (ATCC; CRL-2539TM) spontaneously produces highly metastatic tumors that can metastasize to the lung, liver, lymph nodes, and brain while the primary tumor is growing in situ. Thus, we selected 4 T1 to induce breast cancer model in mice. Subsequently, the mice were divided into CYP-only and CYP + DOX groups. DOX was injected after CYP injection, following which tumor granules emerged. The tumor vanished in the CYP + DOX group, but was harvested from mice in the CYP-only group (Fig. 10).

The right back side hair were shaved on 6 female BALB/c mice and treated with compound cream 40 μ L (2 mg/mL) once every two days. Two mice were sacrificed every week, and two sides of the back skin were collected for H-E staining.

The right back side hair on 2 female BALB/c mice was shaved and treated with compound cream 2000 mg/kg (cream concentration 40%) one time. The mice were observed daily and sacrificed on day 21. The right-side skin was collected for H-E staining.

Two back sides of 5 female BALB/c and C57 mice were depilated with paraffin wax. The right side was treated with compound cream (40 μ L, 2 mg/mL) and the left side with

Fig. 1 Hair follicle stem cells and proliferation from C57BL/6 Mice. Cell proliferation assay: An equivalent of 2×10^3 cells were seeded in 100 μ L volume in 96-well plate. Compound 6b (1, 5, 10, 20, 40 μ M) was diluted with DMEM and assessed by Cell Counting Kit-8 (CCK-8) assay on days 1, 3, 5, and 7 at OD 450 nm



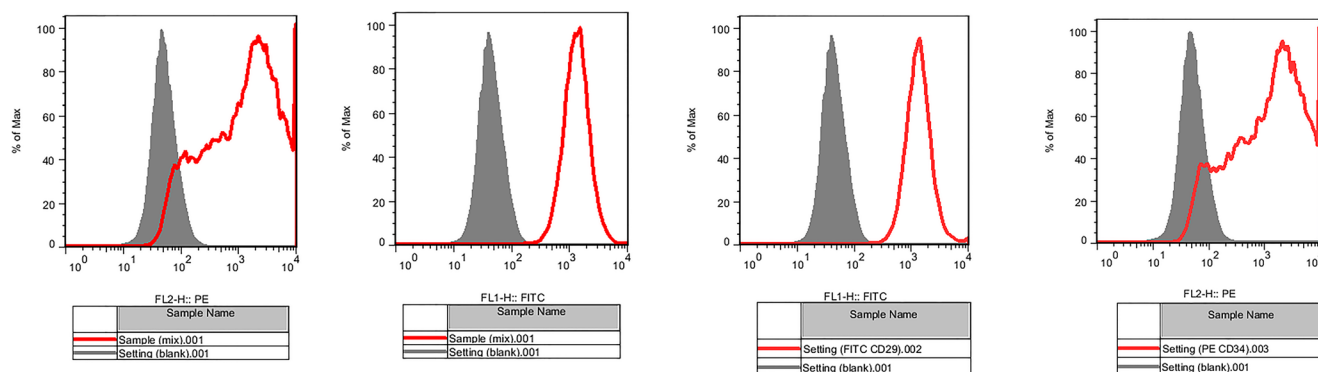


Fig. 2 Identification of hair follicle stem cell. Setting001: Blank; Sample001: FITC/PE [(FITC-anti-mouse $\beta 1$ integrin)/(PE-anti-mouse CD34)]; Setting002: FITC(FITC-anti-mouse $\beta 1$ integrin); Setting003:

PE(PE-anti-mouse CD34). Method: An equivalent of 1×10^5 cells were seeded in 100 μ L staining buffer. PE-anti-mouse CD34 antibody and

control cream (40 μ L) while the mice were injected with CYP (20 μ g/g) one time. The cream treatment was given once per two days. The animals were sacrificed on day 21, and two sides of the back skin were collected for H-E staining. M1 = Mouse 1, M2 = Mouse 2.

Two back sides of 5 female BALB/c and C57 mice were depilated with paraffin wax. The right side was treated with compound cream (40 μ L, 2 mg/mL) and the left side with control cream (40 μ L) while the mice were injected with DOX (15 μ g/g). The cream was treated once per two days; Doxorubicin (5 μ g/g) was injected s.i.d three days after depilation. Mice were sacrificed on day 21, and two sides of the back skin were collected for H-E staining.

4 T1 cells ($1 \times 10^6/100 \mu$ L) were injected into the right side of 10 female BALB/c mice subcutaneously, but no abnormality occurred after 2 days. CYP (150 mg/kg) was injected i.p.

and still no abnormality occurred in 5 days. The left side hair was shaved, and the compound cream was applied. On day 7 after 4 T1 injection, granules emerged on the right skin. On day 11, one group (5 mice) was injected doxorubicin (15 μ g/g). All the mice were sacrificed on day 21; the CYP group mice normally weighed with obvious tumor while the CYP + DOX group mice emaciated in dry hair without tumor on the right side. The two sides of the back skin and tumor pieces were collected for H-E staining.

TLR7-targeted compound designation and selection

To the best of our knowledge, the various effects of TLR7 in infection, inflammation, immune diseases, and tumor were assessed to identify and enrich new TLR7-agonistic structures. The co-crystallization of TLR7 and compound R848 was used as a model to design the targeted compounds according to the protein data bank (PDB code: 5GMH). While virtually screening 432 structures, those containing glycosyl were deleted, and abnormal structures (from SciFinders®) with high scores were selected for the subsequent assays. Finally, 27 compounds with high scores were collected for the following in vitro activity screening.

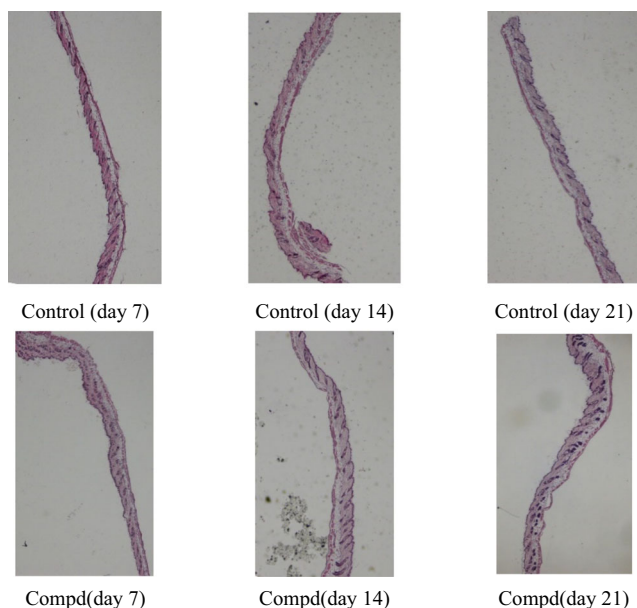


Fig. 3 Compound cream treatment on normal mice

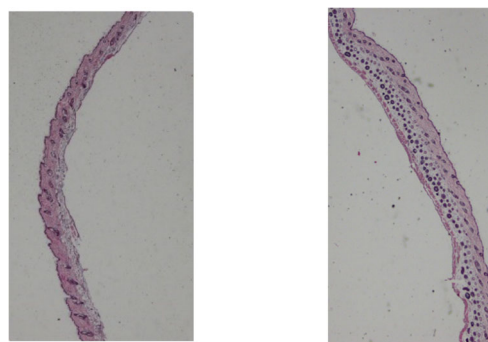
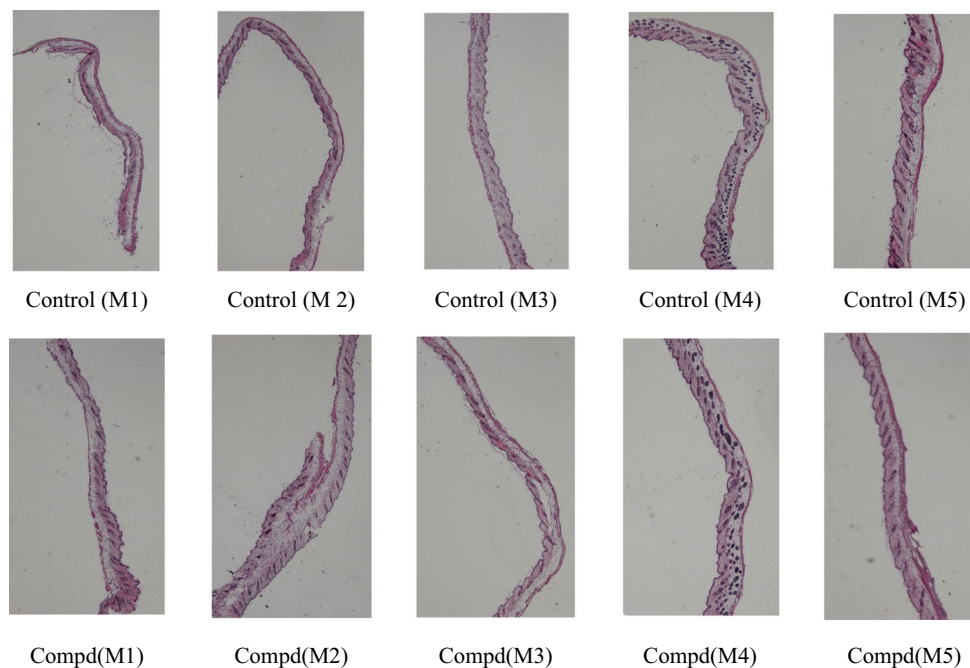


Fig. 4 Acute toxicity

Fig. 5 Compound cream treatment on CYP-injected C57 mice



In vitro assays of virtual screening compounds

TLR7 inhibition activity in HEK 293 cells

The TLR7 agonist activity of all the 27 compounds was evaluated by detecting the HEK-Blue activity in HEK 293 cells expressing TLR7 based on the Quanti-Blue substrate and expressed as a change in the NF- κ B activity. However, no agonists were found in these compounds. Based on the results of inflammation-nitric oxide (NO) inhibition assay, the TLR7 inhibitory activity of

these compounds was tested according to the protocol for TLR9 antagonists [19]. Five compounds (C2, C3, C4, C6, and C7) (Fig. 11) showed steady TLR7 inhibition (Fig. 12).

HEK-BlueTM-hTLR7 cells plated in 96-well plate at a density of 4×10^4 cells/well were stimulated with agonist CL097 (5 μ M) in the presence or absence of these compounds (40 μ M) overnight. The supernatant (20 μ L) was tested with Quanti-blue (OD 630 nm), and the residue was assessed for cell proliferation by CCK-8 method.

$$\text{Index of Quanti-Blue value} = (A-B)/(C-B)$$

where A is the average optical density of the compound-treated cells; B is the average optical density of the control wells (culture medium with only cells); C is the average optical density of the positive control (CL097-treated cells).

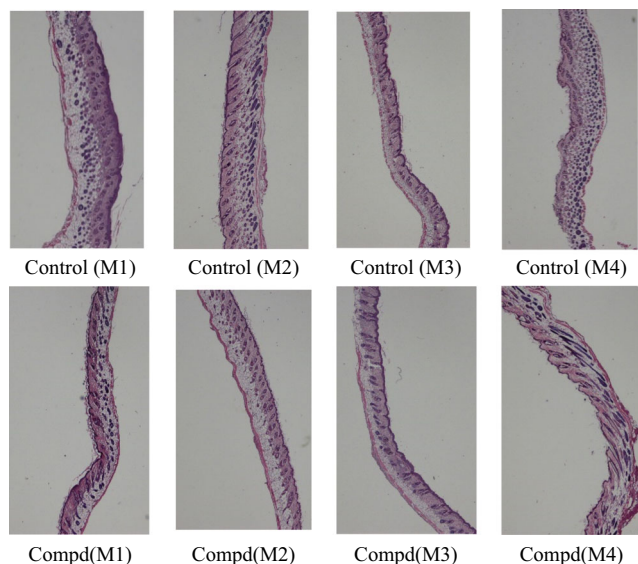


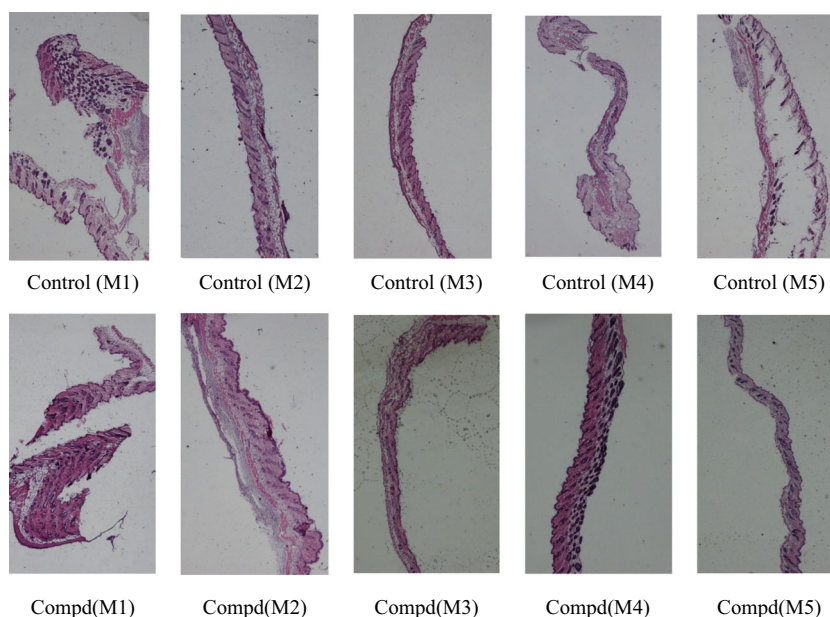
Fig. 6 Compound cream treatment on CYP-injected BALB/c mice

Anti-inflammatory activity in RAW264.7 cells

TLR7 is expressed on airway nerves and mediates the relaxation of human and animal airways through NO production [20]. Also, we evaluated the effects of these 27 compounds on the inhibitory effect of NO on RAW264.7 cells, and the cell viability was determined by MTT assay. Five compounds (C2, C3, C4, C6, and C7) showed anti-inflammatory activity (Fig. 13).

RAW264.7 cells plated in 96-well plate at a density of 4×10^4 cells/well were treated with compounds (40 μ M) and lipopolysaccharide (LPS) (1 μ g/mL, 10 μ L/well) within 1.5 h. The NO concentration was tested using Griess reagent (540 nm) after 24 h in an

Fig. 7 Compound cream treatment on DOX-injected C57 mice



incubator. The cell proliferation was assessed using MTT (200 μ L, 0.5 mg/mL, 450 nm).

$$NO \text{ inhibition rate (\%)} = \frac{LPS-Compound}{LPS-Control} \times 100\%$$

$$Cell \text{ Proliferation (MTT) (\%)} = \frac{Compound - Negative \text{ Control (no cell)}}{Positive \text{ Control (Cell)} - Negative \text{ Control (no cell)}} \times 100\%$$

Ligand-receptor interaction by molecular docking

Herein, we aimed to design the agonist; however, the results indicated that neither did the compounds (C2, C3, C4, C6, and C7) act on TLR7 agonist signaling (NF- κ B pathway) nor present the inflammatory activity like other TLR7 agonists. The antagonistic action of TLR7 was found in the agonist design. To gain a better understanding of the efficiency of the ligand analog molecules, we studied the interaction of the 5 compounds docked into the site of TLR7 receptors.

Fig. 8 Compound cream treatment on DOX-injected BALB/c mice

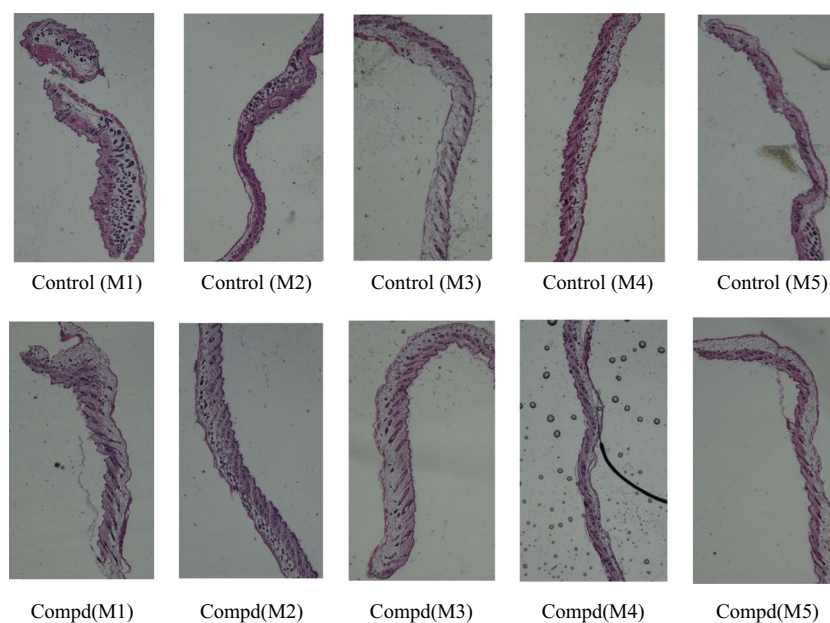
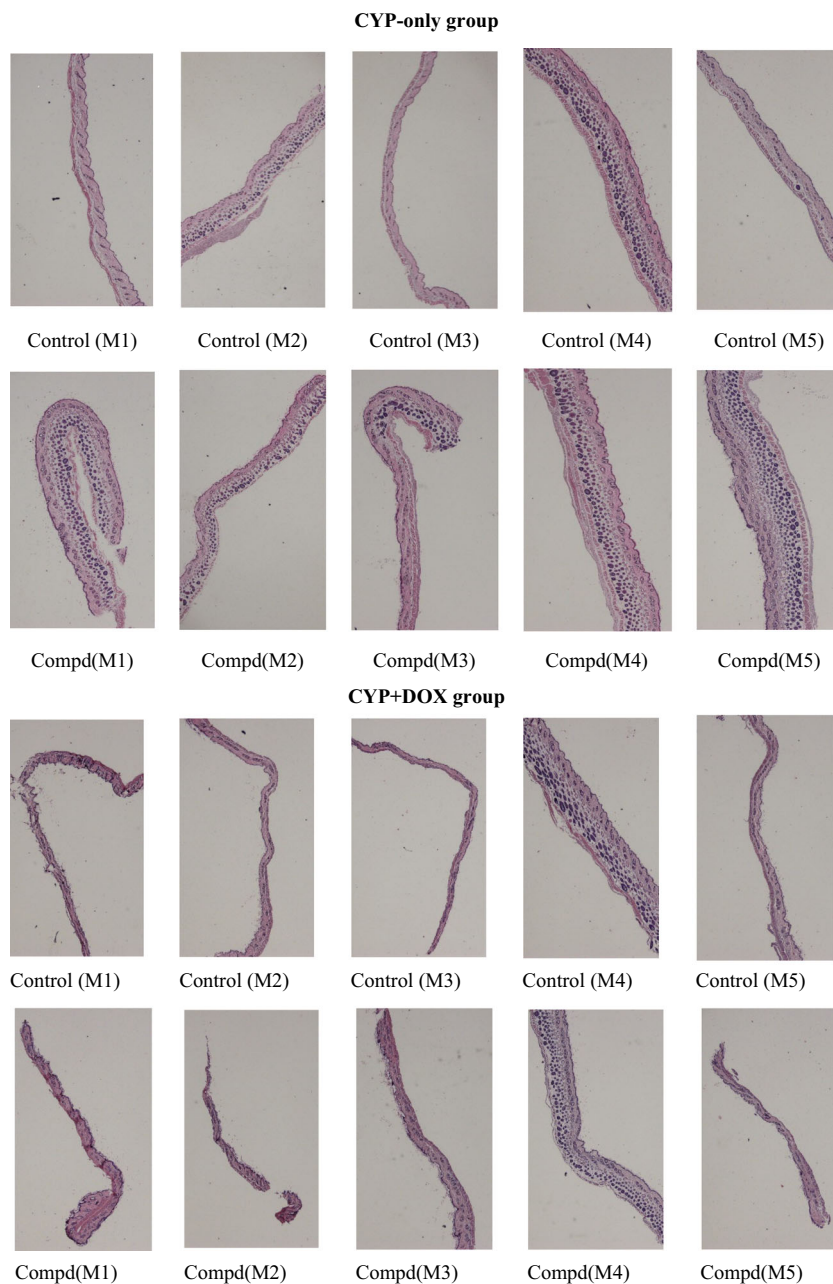


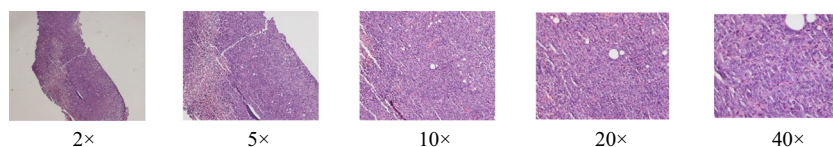
Fig. 9 Compound cream treatment on breast cancer BALB/c mice



Before molecular dockings, the analysis of the first site of TLR7 indicated that the residues Phe408, Asp555, Leu557, Ile585, and Thr586 were directly recognized as first site ligands. The agonistic chemical ligand R848 can form hydrogen bonds with Asp555 and Thr586 and a water bridge with Gly584. The analysis of the binding modes of the five antagonists with TLR7 revealed the first identified site. The first antagonist can form a

strong hydrogen bond with Asp555. In addition, it also forms three arene-H interactions with Ile585 and Thr586. The second antagonist can form two strong hydrogen bonds with Asp555 and Gly584 and two arene-H interactions with Ile585 and Thr586. The third antagonist can form a hydrogen bond with Asp555 and an arene-H interaction with Tyr579. The fourth antagonist can form three hydrogen bonds with the side chains of

Fig. 10 Breast tumor of BALB/c mice from 4 T1 cells



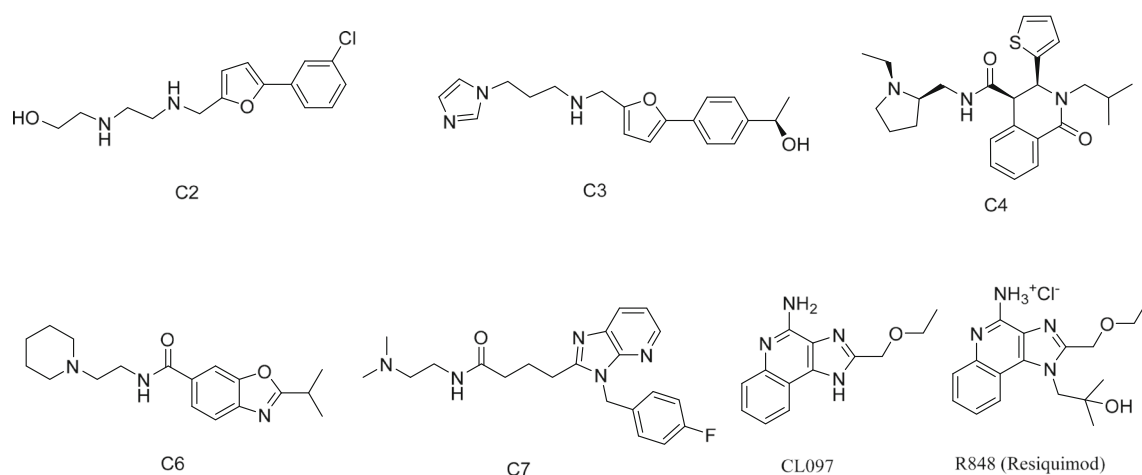


Fig. 11 Antagonistic and agonistic compounds

Asp555 and Thr586. The fifth antagonist can form three strong hydrogen bonds with Asp555, Gln531, and Thr532. In addition, the antagonist can also form an arene-H interaction with the side chain of Ile585. All the five antagonists bound to the TLR7 protein in the same site and formed hydrogen bonds with Asp555, which was critical for the binding of compounds (Fig. 14).

Discussion

Chemotherapy-induced alopecia is a common side effect in cancer treatment [1]. The current treatments of alopecia are not effective for CIA treatment or prevention, and the side effects are not neglected; for example, androgen receptor inhibitors cause feminization and hyposexuality in men. Interestingly, scalp cooling is effective in the clinic [21], and other methods are only partially proved at the preclinical stage [22, 23].

TLR7 is an intracellular toll-like receptor expressed by various cell types. The involvement of TLR7 in the development of autoimmunity has been demonstrated by multiple groups using various approaches [24]. Imiquimod is a toll-like receptor (TLR7/8) agonist that can be applied to mouse skin to elicit

erythema, scaling, keratinocyte proliferation with acanthosis, altered keratinocyte differentiation (parakeratosis), and a dermal infiltrate [25].

The patents of imiquimod are on the rings A, B, C, and the possible branches. The designed compound 6b replaced the atom C with N on ring A and cut the amino-group on ring B. The key process of synthesis was adding different aliphatic amines onto the quinolone ring (step c, Scheme 1). This new structure (6b) avoided all the imiquimod patents successfully and displayed proliferation activity in vitro and in vivo. Of the four synthesized compounds, 6b displayed the lowest values (Table 1) indicating highest hydrophilicity and adequate activity in the in vivo pilot assay.

Strikingly, in the process of expansion of TLR7 agonist structures, 5/27 selectively designed compounds (Fig. 11) displayed TLR7 inhibition in vitro. Conversely, we docked the compounds back to co-crystallization of TLR7 (PDB code: 5GMH). Agonist (R848) combined into TLR7 on the Y-axis direction, tightened the neighboring loop, and formed a triangle to activate the agonist-TLR7 binding protein. Moreover, it could form a dimer system with another TLR7 protein. However, the five antagonists combined on the X-

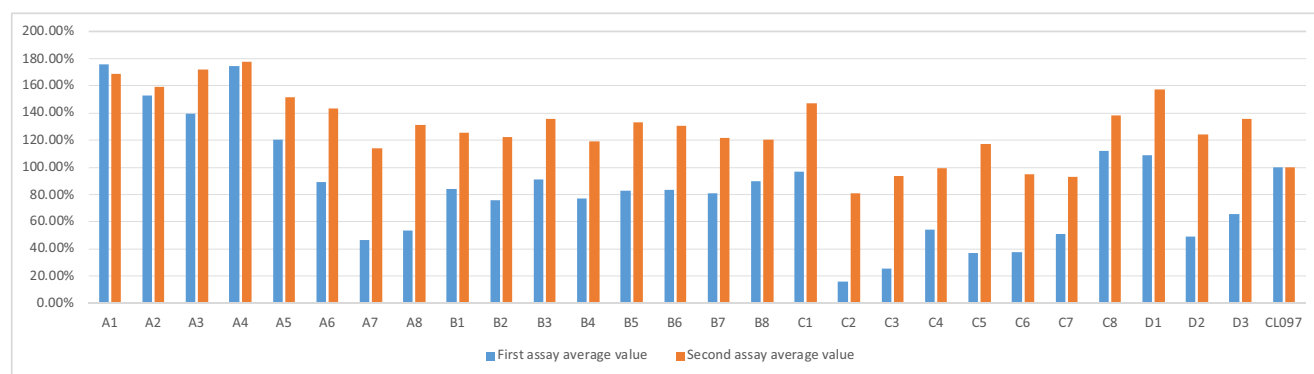


Fig. 12 In vitro TLR7 activity of 27 compounds

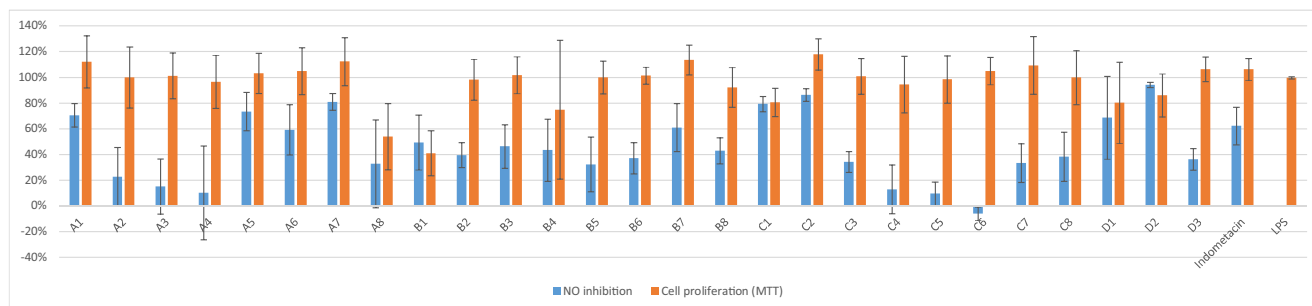
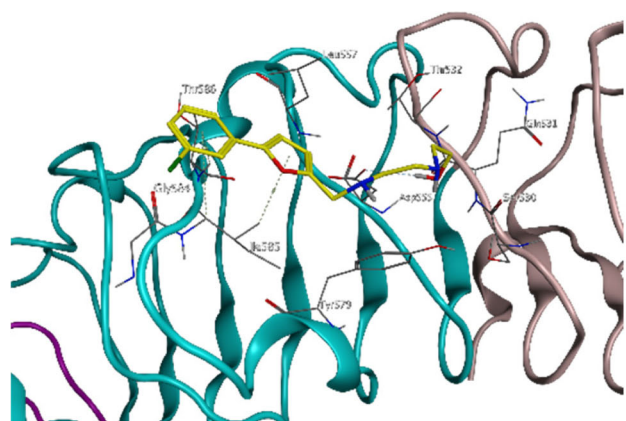


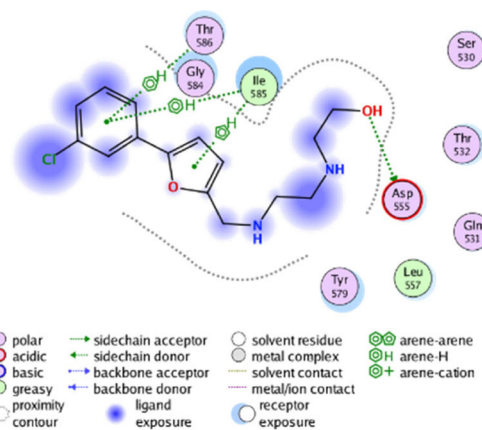
Fig. 13 Effect of compounds on the viability of RAW264.7 cells

axis direction, interacted with neighboring 2–3 TLR7 loops like cap combination mode, and locked onto the first site position. As a result, such conservative combination is difficult for dimer system formation with two TLR7s (Fig. 5). The strong interactions between the five antagonists with TLR7 might induce the conformational changes and affect the binding of the agonistic chemical ligands.

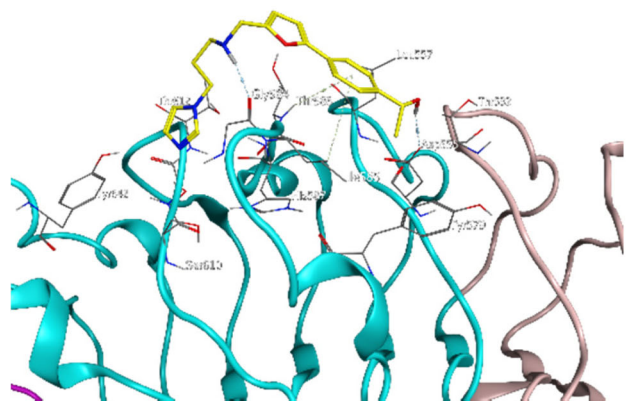
Herein, we designed a series of quinoline derivatives (all unpublished). The derivative synthesis started with aniline, and the key step was replacing the hydroxyl group by various amine groups. One new compound (6b) displayed proliferative activity in vitro and in vivo through branch chain replacement and triazole ring cyclization. The analysis by H-E staining revealed that the size and density of hair follicles on the



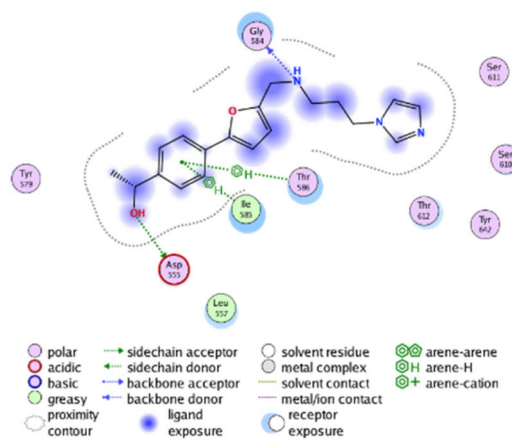
1a. TLR7-antagonist1(Compd C2)



1b. TLR7-antagonist1(Compd C2)_2D

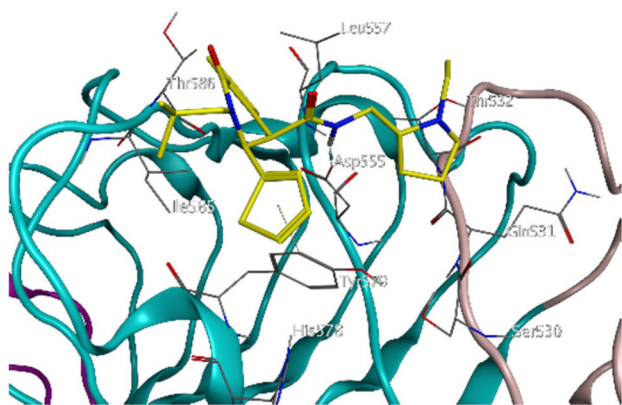


2a. TLR7-antagonist2(Compd C3)

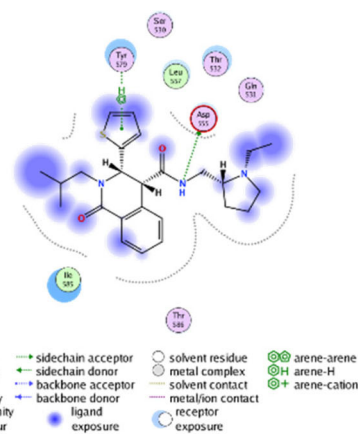


2b. TLR7-antagonist2(Compd C3)_2D

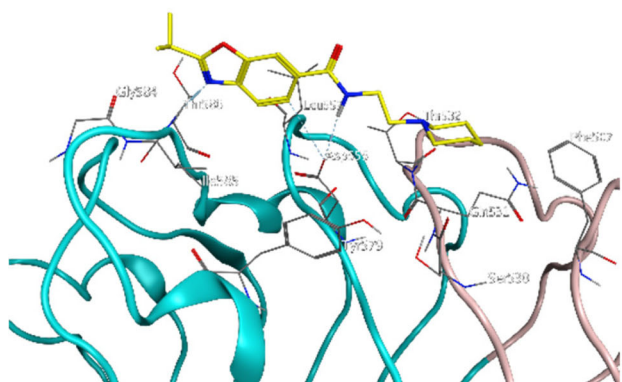
Fig. 14 Ligand-receptor interaction schematic diagrams by molecular docking



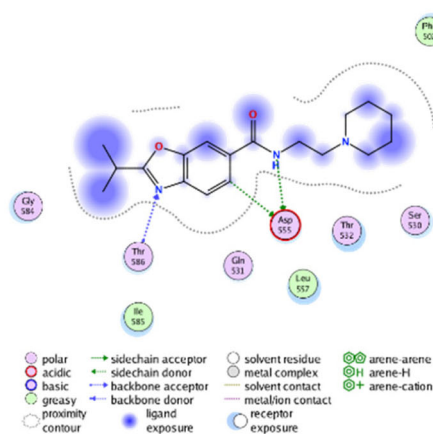
3a. TLR7-antagonist3(Compd C4)



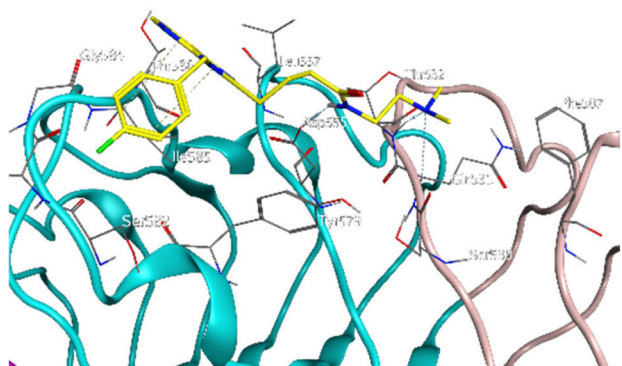
3b. TLR7-antagonist3(Compd C4)_2D



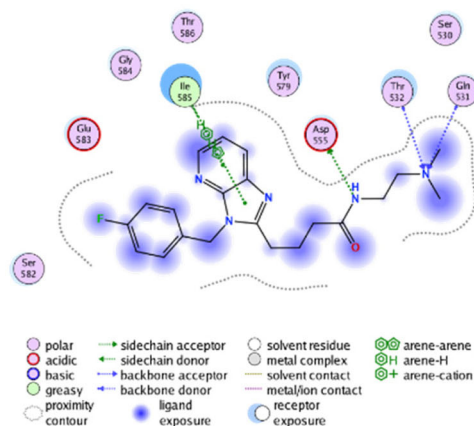
4a. TLR7-antagonist4(Compd C6)



4b. TLR7-antagonist4(Compd C6)_2D



5a. TLR7-antagonist5(Compd C7)



5b. TLR7-antagonist5(Compd C7)_2D

Fig. 14 (continued)

compound-treated groups was larger and thicker than the control groups. Lipophilicity might provide some valuable information on drug design. However, the enzymatic mechanism indicated that 6b was not a TLR7 agonist, and the putative

mechanism is yet to be investigated. A novel series of TLR7 antagonists were designed and discovered. The structural activity correlation studies indicated that combination direction, interaction with neighboring TLR7, and difficulty in the

formation of the dimer system exerted a remarkable effect on the antagonistic activity. Among the five compounds, C6 showed excellent antagonistic activity and NO inhibition activity *in vitro*.

Materials and methods

Compounds synthesis and ointment prescription

Synthesis reagents were obtained from Shanghai Molbase Data Technology Co., Ltd., and Shanghai TopScience Co., Ltd.

Compound cream was prepared from glyceryl monostearate (2%), stearic acid (2%), albolene (5%), paraffin liquid (20%), glycerin (25%), water (40%), SDS (0.9%), borneol (0.5%), DMSO (4.6%), and target compound 6b (100 mg). All the materials were bought from Molbase™. Then, the mixture of components was heated to 80 °C for 0.5 h in a water-bath.

Isolation of mouse hair stem cells

The isolation of mouse hair follicle bulge stem cells was carried out as follows: 10-day-old mice were sacrificed by cervical dislocation. Then, 70% ethanol was added to cover and soak the mice for 5–10 min. The two sides of the tentacle skin were clipped (1.5 × 1.5 cm²). After rinsing with PBS (phosphate-buffered saline), the hair follicles were extracted from the fatty end, and the intact hair follicles were transferred into collagenase I/dispase (1 mg/mL) at 37 °C for 30 min. The connective tissues were removed with a syringe needle, and the hair follicles were cut off. The middle part of the follicle was collected, and skin pieces were transferred into PBS with penicillin and streptomycin and 0.05% trypsin at 37 °C for 10 min. The cells were suspended in DMEM with 10% fetal bovine serum (FBS), and the stem cells were resuspended in complete medium and cultured into 24-well plates.

Cell proliferation was measured using a CCK-8 assay (Dojindo, Kumamoto, Japan) following the manufacturer's instructions, indicating that the compound (6b) promoted cell proliferation at low dosage (1 and 5 μM) in early days (days 3 and 5).

HEK293 cell culture and activity detection

HEK 293 cells (HEK-Blue™-hTLR7 cells, InvivoGen) were maintained in DMEM, 4.5 g/L glucose, 10% (v/v) FBS, 50 U/mL penicillin, 50 μg/mL streptomycin, 100 mg/mL Normocin™, and 2 mM L-glutamine. Cells were cultured at 37 °C in a humidified atmosphere at 5% CO₂; the growth medium was renewed two times a week.

Detection methods: 1) One pouch of QUANTI-Blue™ (InvivoGen) was solubilized into 100 mL sterile water. 2) The QUANTI-Blue™ medium was warmed to 37 °C for 30 min. 3) A volume of 180 μL/well QUANTI-Blue™ medium was dispensed into a flat-bottom 96-well plate. 4) Then, 20 μL of the sample (supernatant of HEK-Blue™-hTLR7 cells with compounds) or negative control was added. 5) The reaction was incubated at 37 °C for 15 min–6 h. 6) The optical density (OD) was measured at 630 nm using a microplate reader.

RAW264.7 cell culture

RAW264.7 cells (Zhejiang Ruyao Biotech, China) were cultured in DMEM medium (supplemented with 10% fetal bovine serum and 1% penicillin/streptomycin) at 37 °C in a humidified atmosphere at 5% CO₂ and seeded into a 96-well plate at a density of 5 × 10⁴ cells/well and incubated for an additional 12 h. Next, different compounds (40 μM) were added, and LPS (1 μg/mL) (Sigma-Aldrich, USA) was added after 1.5 h; the plate was incubated for an additional 24 h.

A volume of 50 μL supernatant was collected for measuring the NO production, using Griess reagent (Beyotime Biotech, China); the OD values were measured at an excitation wavelength of 540 nm.

Subsequently, 200 μL MTT (0.5 mg/mL) was added into the residue and incubated at 37 °C for 4 h. Then, the dark supernatants were removed, the left “black slag” was solubilized in 150 μL DMSO, and OD was measured at 490 nm. Each group of samples was subjected to four parallel experiments.

Hair follicle proliferation activity in mice

Animal study protocols were approved by the Institutional Animal Care and Use Committee at the National Cancer Center (Chinese Academy of Medical Sciences). C57BL/6 and Balb/c mice were purchased from Vital River Laboratory Animal Technology (Beijing, China).

General protocol: After anesthesia by tribromoethanol, the back skin was daubed with liquified wax. The skin hair was removed with solidified wax. On day 9 post-depilation, the chemotherapeutic agent was administered by *i.p.*, and compound cream was daubed on the right back skin and the control cream on the left back skin. On day 21, mice were killed, and the back skin was collected for histological analysis by H-E staining.

Normal mice were treated with compound cream (4 mg/kg) q2d.

Mice exhibiting acute toxicity were treated only one time with high dose compound cream (800 mg/kg).

Chemotherapeutic mice (CYP) were injected 150 mg CYP/kg once, while chemotherapeutic mice (DOX) were injected 5 mg DOX/kg q3d.

Breast cancer mice were injected with 4 T1 cells (1×10^6 /mouse), and chemical doses were administered similarly as chemotherapeutic mice above.

Groups	Day 9	Day 5	Day 3	Day 0	Day 6	Day 7	Day 14	Day 21
1 Normal mice				Depilation+cream		Kill 2	Kill 2	Kill 2
2 Acute toxicity mice				High dose cream				Kill
3 CYP mice	Depilation			CYP + cream				Kill
4 DOX mice	Depilation			DOX + cream				Kill
5 Breast Cancer mice A		Inject 4 T1 cells	CYP	Depilation+cream				Kill
6 Breast Cancer mice B		Inject 4 T1 cells	CYP	Depilation+cream	DOX			Kill

Molecular docking

The agonist-bound TLR7 structure (PDB code: 5GMH, Resolution: 2.2 Å) was obtained from Protein Data Bank. The co-crystallized structure was prepared using Molecular Operating Environment (MOE) 2018.0101 for correcting the structural issues (such as break bond and miss loop); also, hydrogen was added, and the partial charge was estimated. The 2D structures of the five antagonists were converted to 3D in MOE through energy minimization. The MOE dock was used for docking simulation of the antagonists and predicting their binding affinity to the TLR7 protein structure. The original ligand-binding pocket served as the active docking site. A classical triangle match was selected as the placement method, and the number of placement poses was set to 300. The output docking poses were evaluated by the London dG score. Then, the rigid receptor method was employed in the refinement step. The number of the final output docking poses was set to 50 that was minimized using Amber12:EHT force field in MOE. The GBVI/WSA dG score was used to evaluate the binding of the antagonists with the TLR7. Finally, the binding mode was analyzed in MOE after minimizing the structure.

Acknowledgements The key structures have applied Chinese patent. (CN201711279295, CN108003153A).

We thank Zhejiang Ruyao Biotech Co.,LTD for technologic support.

Funding The work was supported by National Natural Science Foundation of China (No. 81603218).

Compliance with ethical standards

Conflict of interest Author Jincheng Yang declares that he has no conflict of interest. Author Kun Chen declares that she has no conflict of interest. Author Bin Wang declares that he has no conflict of interest. Author Liudi Wang declares that she has no conflict of interest. Author Shuya Qi declares that she has no conflict of interest. Author Weihua Wang declares that she has no conflict of interest.

Ethical approval This article does not contain any studies with human participants performed by any of the authors. Animal experiments were approved by the Institutional Animal Care and Use Committee at National Cancer Center, Chinese Academy of Medical Sciences. (NCC2016A050, 9 March 2016) All applicable international, national, and institutional guidelines for the care and use of animals were followed.

References

- Nalluri R, Harries M (2016) Alopecia in general medicine. *Clin Med* 16(1):74–78
- Chen C, Chang Y, Liu H, Chen Y (2018) Cancer risk in patients with alopecia areata: a nationwide population-based matched cohort study. *Cancer Med* 7:2153–2159
- Seo H, Han S, Kim J (2018) Cancer risks among patients with alopecia areata: a population-based case-control study in Korea. *J Am Acad Dermatol* 78:209–211
- Roe H (2011) Chemotherapy-induced alopecia: advice and support for hair loss. *Br J Nurs* 20:S4–S11
- Jayde V, Boughton M, Blomfield P (2013) The experience of chemotherapy-induced alopecia for Australian women with ovarian cancer. *Eur J Cancer Care (Engl)* 22:503–512
- Wang J, Lu Z, Au LS (2006) Protection against chemotherapy-induced alopecia. *Pharm Res (Dordrecht)* 23(11):2505–2514
- Trüeb RM (2009) Chemotherapy-induced alopecia. *Semin Cutan Med Surg* 28(1):11–14
- Panteleyev A (2018) Functional anatomy of the hair follicle: the secondary hair germ. *Exp Dermatol* 27:701–720
- Chen R, Miao Y, Hu Z (2019) Dynamic nestin expression during hair follicle maturation and the normal hair cycle. *Mol Med Rep* 19(1):549–554
- Ralf P, Haslam Iain S, Sharov Andrey A et al (2013) Pathobiology of chemotherapy-induced hair loss. *Lancet Oncol* 14:e50–e59
- Amberg N, Holcman M, Stulnig G, Sibilia M (2016) Effects of Imiquimod on hair follicle stem cells and hair cycle progression. *J Invest Dermatol* 136(11):2140–2149
- Letada PR, Sparling JD, Norwood C (2007) Imiquimod in the treatment of alopecia universalis. *Cutis* 79(2):138–140
- Paus R, Cotsarelis G (1999) The biology of hair follicles. *N Engl J Med* 341(7):491–497

14. Kontogiorgis CA, Hadjipavloulitina DJ (2017) Synthesis and antiinflammatory activity of coumarin derivatives. *J Med Chem* 48(20):6400–6408
15. Zheng Y, Hsieh J-C, Escandon J, Cotsarelis G (2016) Isolation of mouse hair follicle bulge stem cells and their functional analysis in a reconstitution assay. *Methods Mol Biol Chapter 8*. 1453:57–69
16. Ma DR, Yang EN, Lee ST (2004) A review: the location, molecular characterisation and multipotency of hair follicle epidermal stem cells. *Ann. Acad. Med. Singap* 33:784–788
17. Meihua G, Pan Z, Chunyang L et al (2018) Protective mechanism of adipose-derived stem cells in Remodelling of the skin stem cell niche during Photoaging. *Cell Physiol Biochem* 51:2456–2471
18. Sasaki S, Baba T, Muranaka H, Tanabe Y, Takahashi C, Matsugo S, Mukaida N (2018) Involvement of prokineticin 2-expressing neutrophil infiltration in 5-fluorouracil-induced aggravation of breast cancer metastasis to lung. *Mol Cancer Ther* 17:1515–1525
19. Wang D, Bhagat L, Yu D, Zhu FG, Tang JX, Kandimalla ER, Agrawal S (2009) Oligodeoxyribonucleotide-based antagonists for toll-like receptors 7 and 9. *J Med Chem* 52(2):551–558
20. Drake M, Scott G, Proskocil B et al (2013) Toll-like receptor 7 rapidly relaxes human airways. *Am J Respir Crit Care Med* 188(6):664–672
21. Young A, Arif A (2016) The use of scalp cooling for chemotherapy-induced hair loss. *Br J Nurs* 25:S22–S27
22. Katikaneni R, Ponnappakkam T, Matsushita O, Sakon J, Gensure R (2014) Treatment and prevention of chemotherapy-induced alopecia with PTH-CBD, a collagen-targeted parathyroid hormone analog, in a non-depilated mouse model. *Anti-Cancer Drugs* 25(1):30–38
23. Belen R-G, Margit J, Jamie F et al (2018) Pathogenesis and treatment options for chemotherapy-induced alopecia: a systematic review. *Int J Dermatol* 57:1417–1424
24. Rubtsova K, Marrack P, Rubtsov AV (2015) TLR7, IFN γ , and Tbet: their roles in the development of ABCs in female-biased autoimmunity. *Cell Immunol* 294(2):80–83
25. Swindell William R, Michaels Kellie A, Sutter Andrew J et al (2017) Imiquimod has strain-dependent effects in mice and does not uniquely model human psoriasis. *Genome Med* 9:24

Publisher's note Springer Nature remains neutral with regard to jurisdictional claims in published maps and institutional affiliations.